Publications of the Astronomical Society of the Pacific
108: 500–509, 1996 June

Attaining Doppler Precision of 3 m s^{-1} [1,2]

R. PAUL BUTLER,[3] GEOFFREY W. MARCY,[3] ERIC WILLIAMS, CHRIS MCCARTHY,[4] AND PREET DOSANJH

Department of Physics and Astronomy, San Francisco State University, San Francisco, California 94132
Electronic mail: paul@further.berkeley.edu

STEVEN S. VOGT

Lick Observatory and Board of Studies in Astronomy and Astrophysics, University of California, Santa Cruz, California 95064

Received 1996 January 2; accepted 1996 March 22

ABSTRACT. Current spectroscopic techniques yield Doppler-shift errors of 10 to 50 m s^{-1}, barely adequate to detect reflex velocities caused by Jupiter-like and lower-mass planets. We describe a technique which yields relative radial-velocity errors of 3 m s^{-1}. This technique makes use of a fast echelle spectrograph at resolution of R=62,000 and a large-format CCD which acquires the entire visible and near-IR spectrum in each exposure. Starlight is sent through an iodine absorption cell placed at the spectrometer entrance slit. The resulting superimposed iodine lines provide a fiducial wavelength scale against which to measure radial-velocity shifts. The shapes of iodine lines convey the PSF of the spectrometer to account for changes in spectrometer optics and illumination on all time scales. We construct a model of each observed spectrum by multiplying a stellar spectrum with an iodine spectrum and convolving the result with the spectrometer PSF. The free parameters of the model include the wavelength scale, spectrometer PSF, and stellar Doppler shift. All model parameters are derived anew for each exposure and the synthesis is done on a grid of CCD sub-pixels, using spline functions as interpolation predictors. We present Doppler tests of the Sun, τ Ceti, and 107 Psc, observed with the Lick and Keck echelles. All exhibit apparent errors of about 3 m s^{-1}, maintained on time scales of minutes to a year. This precision agrees with the theoretically predicted errors that stem primarily from photon statistics.

1. INTRODUCTION

Traditional astronomical methods of measuring radial velocity typically carry errors of ~1 km s^{-1} or more, making it historically impossible to search for sub-stellar companions around low-mass stars via the Doppler-reflex motion of the primary. For example, Jupiter imparts a velocity of 0.0124 km s^{-1} on the Sun. Griffin and Griffin (1973) suggested that the systematic errors of radial-velocity measurements could be significantly reduced if the reference spectrum were obtained simultaneously with the stellar spectrum. They proposed using the absorption lines that are superimposed by the (nearly stationary) Earth's atmosphere (telluric). Modern versions of this suggestion replace the telluric reference lines with those from a chemical absorption cell or a stabilized Fabry–Perot etalon interferometer.

Within the last 15 years a number of groups have achieved a long-term velocity precision of 15 m s^{-1} or better (Campbell and Walker 1988; Marcy and Butler 1992; McMillan et al. 1994; Cochran and Hatzes 1994; Brown et al. 1995). The work of the longest duration (Campbell et al. 1988; Walker et al. 1995) provided startling constraints on the occurrence of planets. With a 12-year baseline covering 21 solar-type stars at a precision of ~15 m s^{-1}, they report no evidence for the existence of sub-stellar companions though they clearly would have detected planets down to ~2 Jupiter masses. This implies that at most only 5% of solar-type stars have planets larger than twice Jupiter's mass within 5 AU.

The results of the Campbell and Walker survey suggest two strategies for subsequent Doppler-reflex planet search efforts. First, an attempt to significantly improve velocity precision should be made in order to search for sub-Jovian planets. For example, Saturn imparts a velocity of 2.7 m s^{-1} on the Sun. This paper represents such an effort. Second, non-solar-type stars (late-K and M dwarfs) should be investigated. A few such stars are being observed, but most late-K and M dwarfs are fainter than 8th magnitude, thus requiring a 10-m class telescope.

Ultimately the limit to velocity precision is set by the stars themselves. On long time scales stellar magnetic cycles, analogous to the solar cycle, could insidiously cause an apparent periodic change in radial velocity (Jimenez et al. 1986; Deming et al. 1987). The results of Campbell and Walker demonstrate that this effect must be smaller than 10 m s^{-1} for solar-type stars. For the Sun itself, McMillan et al. (1993) have shown that over a 5-year period the measured radial-velocity variations are no more than 4 m s^{-1}. If the Sun is a typical dwarf star, then intrinsic stellar radial-velocity variations will not mask the presence of a Saturn-like planet.

[1]Based on observations obtained at the W. M. Keck Observatory, which is operated jointly by the University of California and the Californian Institute of Technology.
[2]Based on observations obtained at Lick Observatory, which is operated by the University of California.
[3]Also at Department of Astronomy, University of California, Berkeley, CA 94720.
[4]Currently at Department of Astronomy, University of California at Los Angeles.

Other applications of precise velocities include the search for stellar pulsation modes similar to the 5-minute solar oscillation (asteroseismology), the search for small-amplitude variables (Butler 1992), the detection of photospheric velocity gradients in Cepheids (Butler 1993), and the search for pulsational modes throughout the H-R diagram (Hatzes and Cochran 1995). Section 2 will detail a technique for obtaining radial velocities at a precision of 3 m s^{-1}. Errors will be discussed in Sec. 3. Radial-velocity results will be presented in Sec. 4. Future improvements will be discussed in Sec. 5.

2. PRECISION RADIAL VELOCITIES

Errors in radial velocity stem from spatial and temporal differences in the way that the stellar and reference spectra are obtained. The stellar beam is collected and focused by the telescope and typically contains shadows from the secondary mirror and supports. This beam unevenly overfills the spectrograph slit and wanders about due to guiding errors and atmospheric refraction. Fiber-optic scramblers reduce this instability in illumination (Ramsey 1987). In contrast, the beam from the comparison lamp usually does not pass through the telescope optics and hence traverses a path through the spectrograph that is slightly different from that of the starlight. It encounters the lenses, mirrors, prisms, and gratings in slightly different locations so that zonal variations in optical performance cause spurious changes in the final destination and PSF of each wavelength (Marcy and Butler 1992; Brown et al. 1995).

The stellar and reference spectra also differ in that they are taken at different times. Over time, spectrometers are subject to flexure, relaxation, and thermal expansion, as well as changes in air pressure. These effects produce spectrograph zero-point shifts in wavelength scales and changes in dispersion. A reference spectrum obtained immediately before and after a stellar exposure cannot fully account for these changes. These problems are overcome by simultaneously obtaining the stellar and reference spectra. The following subsections will describe the iodine absorption cell technique.

2.1 Observational Technique

In 1987 the Lick Iodine Planet Search began by making use of the "Hamilton" spectrometer (Vogt 1987), a large-format cross-dispersed echelle that captures the entire visible and near-IR spectrum at resolution of $R=62{,}000$. The Hamilton is fed by both the 3-m Shane (at Coudé focus) and the 0.6-m Coudé Auxiliary (CAT) Telescopes, and both are routinely used for precise velocity work with no difference in velocity zero point. This iodine absorption-cell technique has also been carried out on the HIRES spectrometer (Vogt et al. 1994) during a Keck engineering run.

To maximize the useful wavelength coverage, a literature and laboratory search was made to find an ideal absorption-cell molecule. Such a molecule must be stable and produce many sharp features over the 4000 to 6000 Å region where most of the stellar radial-velocity information resides for late-type stars (Merline 1985). It is also desirable that the absorption-cell molecule be non-lethal. Molecular iodine was chosen as the best overall compromise (Marcy and Butler 1992; Libbrecht and Peri 1995; Butler 1987; Koch and Wohl 1984), providing wavelength coverage from 5000 to 6200 Å.

The chief advantage of the iodine technique is that a S/N ratio of 200 is sufficient to achieve a precision of 3 m s^{-1}, requiring a 10-min exposure for a $V=5$ star on the 3-m Shane Telescope. This throughput has enabled the program to undertake a large survey of 120 late-type stars (F, G, K, and M).

In 1994 November the Schmidt camera optics of the Hamiltonian spectrometer were upgraded with a corrector and field flattener. The intrinsic resolution ($R=\lambda/\Delta\lambda$) of the spectrograph was improved from 40,000 to 120,000. Prior to this upgrade, the spectrograph PSF had been quite asymmetric and varied significantly over the CCD format. In the current "post-fix" era, the one-dimensional point-spread function (PSF) of the Hamilton is quite symmetric and varies little (a few percent) over the CCD format. This has led to achieving radial-velocity precision of 3 m s^{-1} over the last year.

The construction of the iodine cell is described elsewhere in detail (Marcy and Butler 1992; Butler 1987). The cell is 10 cm in length and 5 cm in diameter and contains ~0.001 Atm of iodine. A temperature controller maintains the absorption-cell temperature at 50±0.1 °C. At this temperature the iodine exists as a molecular gas. The cell is mounted directly in front of the spectrograph slit in the converging *f*/36 telescope beam. Starlight passes through the cell just prior to entering the spectrograph slit. The iodine cell thus acts as a transmission filter, imposing thousands of extremely sharp lines on the starlight.

A permanent circular mask with a central obstruction is placed over the spectrograph collimating mirror, centered on the optical axis of the telescope beam. The central obstruction matches the location of the shadow of the telescope secondary mirror. This guarantees that calibration lamps will illuminate the same section of the collimator as the telescope beam. Great care is taken in focusing the spectrograph. A thorium–argon lamp is used to produce approximately 50 strong unblended thorium lines which have been chosen to cover the full range of the 16 echelle orders that contain significant iodine information. The width of each thorium line is determined by a Gaussian fit, and a mean linewidth is determined at several focus positions, with best focus being the location at which the mean linewidth is minimized.

The photon-weighted midpoint of each observation is determined by means of a rotating "fan-blade" mirror which directs about 2% of the stellar beam to a photomultiplier which is connected to a dedicated PC. This mid-time must be known to better than 30 s to guarantee that errors in the barycentric correction to the Earth's motion be kept under 1 m s^{-1}. Tests indicate that the actual midpoints of observation are determined to within 10 s.

2.2 Modeling the Observations

A photon-limited Doppler analysis must consist of a full model of the spectroscopic observation. Instrumental effects

that must be considered include shifts in the spectrograph wavelength zero point, changes in the spectrograph dispersion, and distortions of the instrumental profile or 1D PSF of the spectrometer. The observation is modeled as the product of two functions, the intrinsic stellar spectrum, I_s, and the transmission function of the iodine absorption cell, T_{I2}. This product is then convolved with the spectrograph PSF and binned to the wavelength extent of the CCD pixels. The entire spectrum from 5019 to 5872 Å, which consists of 16 echelle orders spread over 30,000 pixels, is included in the Doppler analysis, broken into chunks of length ~2 Å.

Spectra taken through the iodine cell, $I_{\rm obs}$, are modeled as

$$I_{\rm obs}(\lambda)=k[T_{I2}(\lambda)I_s(\lambda+\Delta\lambda)]*{\rm PSF}, \quad (1)$$

where k is a normalization factor, $\Delta\lambda$ is the Doppler shift, PSF is the spectrograph point-spread function, and "*" represents convolution.

The modeling process requires two input functions, T_{I2} and I_s. The iodine cell transmission function, T_{I2}, was directly measured at the Kitt Peak National Observatory using the Fourier Transform Spectrometer (FTS) at the McMath Solar Telescope on 1995 October 9. The resolution of this spectrum is $\lambda/\Delta\lambda=10^6$ and the S/N ratio is 700. This spectrum is fully resolved and oversampled, compared with the usual characteristics of astronomical echelles. The FTS provides an absolute vacuum wavelength scale accurate to 1 part in 10^8, and even higher internal precision.

The intrinsic stellar spectrum, I_s, is somewhat more difficult to obtain, since it must have high resolution and high S/N ratio. Unfortunately the 0.9-m FTS of the McMath Telescope is unable to take spectra of stars fainter than 1st magnitude. Instead we generate I_s from extremely high S/N (~500) observations taken with the Lick 3-m or CAT and the Hamilton spectrometer. These reference stellar spectra contain smearing from the spectrometer PSF, and therefore cannot serve as I_s. A deconvolution of the PSF is performed as follows. Observations of extremely bright rapidly rotating B stars are made through the iodine absorption cell just before and after the stellar reference observation. The spectrum of these B stars is essentially featureless so, after passing through the iodine absorption cell, they simply convey the absorption spectrum of molecular iodine. The B stars thus act as stellar incandescent lamps with the advantage that they illuminate all the telescope and spectrometer optics in just the same way that the stellar observations do. The PSF of the spectrometer is then calculated by comparing the B-star iodine observations to the reference FTS iodine atlas, T_{I2}, as described in Valenti et al. (1995). This PSF derived from the B-star iodine is then used to deconvolve the PSF out of the template stellar observations. The deconvolution is carried out using a modified Jansson technique (Gilliland et al. 1992).

The modeling process is described in detail by Valenti et al. (1995). The only difference here is the inclusion of the stellar spectrum and its variable Doppler shift. Functionally, each observation is broken up into several hundred 40-pixel (2 Å) chunks. To preserve the high-frequency information of the iodine spectrum (Fig. 1), the synthetic spectrum is calculated at four times the observed sampling (4 model pixels per observed pixel). The wavelength scale of the model is described by two parameters, a wavelength zero point and a linear dispersion, with the zero point defined at the center of the 40-pixel chunk to enhance "orthogonality." The FTS iodine spectrum is then resampled to the same wavelength scale (4×oversampled) by using a spline function for interpolation.

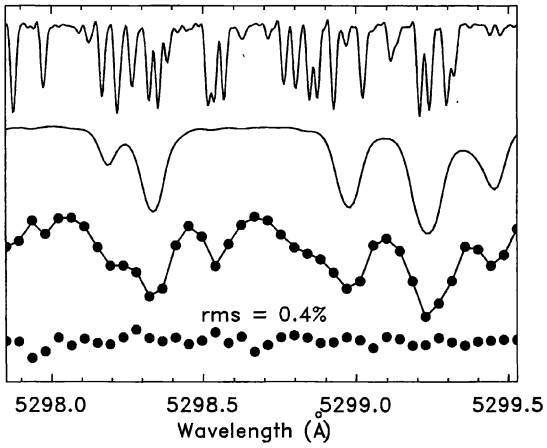

FIG. 1—The modeling process. Top: The template iodine cell spectrum. Second: The template stellar spectrum (τ Ceti, G8 V). Third: The points are an observation of τ Ceti made through the iodine absorption. The solid line is a model of the observation. The model is composed of the template iodine and stellar spectra. The free parameters consist of the spectrograph PSF and the Doppler shift of the template star relative to the template iodine. Bottom: 10 times the difference between the model and the observation. The model and observation differ by 0.4% rms.

The Doppler shift of the stellar spectrum is represented by a single parameter: $z(=\Delta\lambda/\lambda)$. The Doppler shift is accomplished by "splining" the (deconvolved) template stellar spectrum onto the Doppler-shifted wavelength scale. We have performed extensive tests of alternative interpolation schemes, including some that explicitly preserve spectrophotometric integrity, but have concluded that spline functions supply adequate accuracy when working with 4× oversampled pixels. The shifted stellar spectrum is multiplied by the iodine spectrum, and then convolved with the PSF. The convolution is accomplished by a straightforward numerical multiplication of the spectrum with the PSF, carried out at a range of offsets. The PSF description is given by the sum of 11 Gaussians that have fixed positions and widths but variable heights. These Gaussians are placed at intervals of half an observed pixel, and they have widths (σ) of 0.3 an observed pixel. The height of the central Gaussian is fixed at unity, and its Gaussian width is fixed at σ=0.4 pixels. This PSF description thus requires one parameter for each Gaussian that sits "off center." In total this model requires 13 parameters, 2 for the wavelength scale, 1 for the Doppler shift, and 10 for the PSF description. Finally, the synthetic spectrum is binned to pixels that match the observed CCD pixels. The 13 parameters are determined by comparing the model to the observation using a standard "Marquardt" nonlinear least-squares algorithm (Press et al. 1986).

An example of the modeling process is shown in Fig. 1. The top panel shows the transmission function of the iodine absorption cell (T_{I2}) as determined by the FTS. The second panel shows the intrinsic spectrum (I_s) of the bright star τ Ceti (HR 509). The dotted points in the third panel show an actual observation of τ Ceti taken through the iodine absorption cell with the Hamilton spectrograph. The solid line in the third panel is the model of the observation constructed from the two input functions, T_{I2} and I_s, convolved by the derived spectrograph PSF. The bottom plot shows ten times the differences between the model and the observation. The rms difference between model and the observation is 0.4%, consistent with the photon-shot noise in the observation of 0.3%.

The resulting "best-fit" Doppler shift is corrected to the Solar System barycenter. We use a routine written by one of us (C.M.) which is based on the Jet Propulsion Laboratory Solar System ephemeris (Standish et al. 1995; Standish 1990). The barycentric velocity correction includes the following effects, all important at a level about 1 m s^{-1}: velocity vector of observatory relative to the solar system barycenter, time dilation, general relativistic blueshift due to solar gravitational potential field, modification of stellar coordinates due to proper motion, and the apparent secular acceleration due to transverse component of the stellar velocity vector (McCarthy 1995). The flux-weighted midpoint of each observation is determined during each exposure and is adopted as the fiducial "time of the exposure." The resulting barycentric corrections are precise to within 0.1 m s^{-1}.

3. ERROR ANALYSIS

Several sources of error, both experimental and astrophysical, will be discussed in this section. The experimental errors include photon-limited (noise) errors, wavelength calibration, spectrometer PSF, and CCD inhomogeneities. The primary source of astrophysical error that will be considered here is photospheric turbulence.

3.1 Photon-Limited Errors

We compute here the error in the radial-velocity measurement, due entirely to the photon statistics of the acquired spectrum. Each pixel, i, contributes some Doppler-shift measurement, V_i, and contributes some error σ_{V_i}. In practice, we implicitly determine the weighted Doppler shift of an entire "chunk" of spectrum. We may compute the average velocity, $\bar{V}$, of a chunk, and its photon-limited error, $\sigma_{\bar{V}}$. The error in the mean of many measurements (all of the included pixels), that each carry Gaussian distributed errors, is given by Taylor (1982);

$$\sigma_{\bar{V}} = \sqrt{\sum \left(\frac{\partial \bar{V}}{\partial V_i} \sigma_{V_i} \right)^2}. \quad (2)$$

The uncertainty in the mean, $\sigma_{\bar{V}}$, is the sum in quadrature of the velocity errors from each pixel σ_{V_i}, weighted by the sensitivity of the resulting mean velocity to each pixel $\partial \bar{V}/\partial V_i$.

The mean velocity of a chunk, $\bar{V}$, is the weighted mean of the velocities from all pixels in the chunk. We adopt pixel weights given by $w_i = 1/\sigma_{V_i}^2$, where σ_{V_i} is the error in the Doppler velocity contributed by each pixel alone (determined below). Thus, since the weighted mean chunk velocity is

$$\bar{V} = \frac{\Sigma w_i V_i}{\Sigma w_i},$$

the needed partial derivative follows:

$$\frac{\partial \bar{V}}{\partial V_i} = \frac{w_i}{\Sigma w_i}. \quad (3)$$

Substituting Eq. (3) into Eq. (2),

$$\sigma_{\bar{V}} = \frac{1}{\sqrt{\Sigma (1/\sigma_{V_i}^2)}}. \quad (4)$$

This is the error in the mean, for the case in which each pixel contributes a different velocity uncertainty, σ_{V_i}. For the common case of equal uncertainty, this expression reverts to $\sigma_{\bar{V}} = \sigma_{V_i}/\sqrt{N_{\rm pix}}$.

To evaluate the error in the mean velocity from Eq. (4), we need the velocity uncertainty contributed by each pixel, σ_{V_i}. Consider a pixel at which the slope of the residual intensity (continuum at unity) is dI/dV, where dV represents a differential increment in wavelength, in equivalent velocity units. Geometrically, the uncertainty in the velocity from just one pixel, i, is

$$\sigma_{V_i} = \frac{\epsilon_I}{dI/dV}, \quad (5)$$

where ϵ_I is the uncertainty in the residual intensity at pixel i, and dI/dV is the local slope.

Combining Eqs. (4) and (5) gives

$$\sigma_{\bar{V}} = \frac{1}{\sqrt{\Sigma \left(\frac{dI/dV}{\epsilon_I} \right)^2}}. \quad (6)$$

This is the intrinsic Doppler error in any portion of a spectrum, where the sum is over all pixels within that portion. Note that the derivative, dI/dV, represents the slope obtained by the spectrometer, and thus includes instrumental smearing as well as smearing of astrophysical origin. In the case that photon statistics dominate the spectrophotometric error, we have $\epsilon_I = \sqrt{N_{\rm ph}}/N_{\rm ph}$, namely, the fractional Poisson error in the number of photons that arrive in pixel i.

We may consider the example of the steep sides of an absorption line in a solar-type spectrum. The residual intensity varies by roughly ~0.2 within a wavelength span of 2.5 km s^{-1} in lines of moderate strength, so $dI/dV \approx 0.2/2500$ m s^{-1}. From Eq. (6), the observed slopes determine the precision with which shifts can be determined, given noise in the spectrum. We consider a typical special case of S/N=200 in the continuum (40,000 photons). In the steep sides of a line wing where, say, I=0.5, photon statistics gives ϵ_I=0.007. There, Eq. (5) gives $\sigma_{V_i} = 0.007/(0.2/2500) = 88$

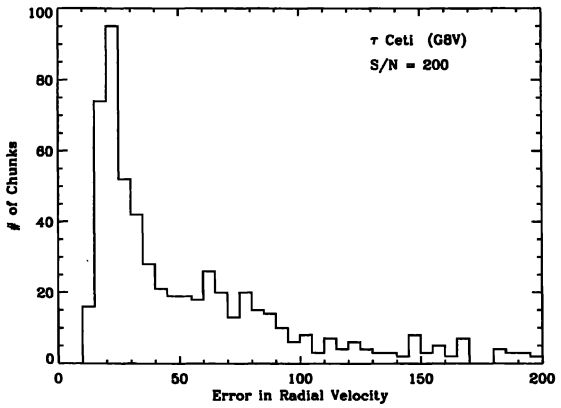

FIG. 2—Histogram of expected errors in all 704 chunks of the spectrum of τ Ceti for S/N=200. Errors are those due to photon statistics only in the stellar spectrum, and are computed from Eq. (6). The peak from 10 to 35 m s^{-1} consists of 230 spectrum chunks which carry the bulk of the precision Doppler information.

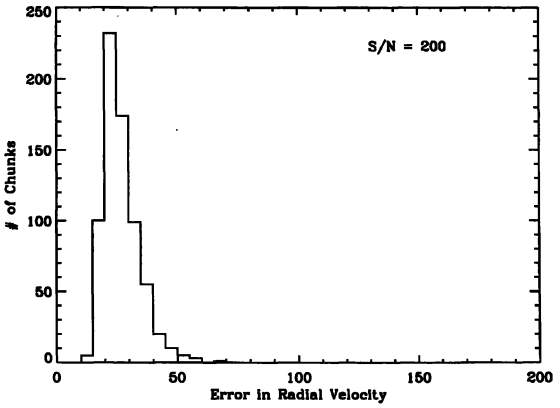

FIG. 3—Histogram of velocity errors due to errors in wavelength calibration from iodine. All 704 chunks of the iodine spectrum are represented for S/N=200. Errors are those due to photon statistics only in the iodine spectrum, and are computed from Eq. (6). The peak from 20 to 40 m s^{-1} consists of 550 spectrum chunks, showing that most chunks have their wavelengths determined with precision of ~30 m s^{-1}.

m s^{-1} for the Doppler-shift error for that pixel. For N such pixels, the error in the mean velocity is $88/\sqrt{N}$. A typical solar absorption line contains ~6 points at typical echelle sampling, yielding a precision of 36 m s^{-1} per absorption line. Clearly, 100 such absorption lines would yield a final velocity error reduced by 10, to 3.6 m s^{-1}. We have checked the above error analysis by Monte-Carlo simulation of spectra with noise artificially introduced, which are then fit with noise-free spectra, leaving the Doppler shift as the free parameter. These numerical tests give resulting errors in excellent agreement with Eq. (6).

Figure 2 shows the histogram of photon-limited Doppler errors for all 704 of the 2-Å chunks in the spectra of τ Ceti (G8 V) obtained at the Lick Observatory echelle. The main peak represents 230 spectrum chunks that each individually yield the Doppler shift with a precision of ~25 m s^{-1}. This implies that the final precision for all chunks is $25/\sqrt{230}=1.6$ m s^{-1}. By including all 704 spectrum chunks, the error in the mean velocity found from Eq. (6) becomes

$$\sigma_{\bar{V}}=1.2 \text{ m s}^{-1}.$$

Thus, 1.2 m s^{-1} is the ultimate precision achievable with the present technique from one exposure of a G-type main-sequence star with the Lick Observatory Hamilton spectrometer for S/N=200. Of course, this error estimate pertains only to stars of spectral type near G8 V that suffer no other significant sources of line broadening, such as due to rotation. For comparison, Tim Brown (private communication 1994) and Horner et al. (1993) analyzed the Doppler content of spectra that have similar wavelength extent and resolution. Both report an expected final Doppler precision of 1 m s^{-1}, similar to that here. Similarly, Hearnshaw (1992) reports that the photon-limited Doppler error is 4.2 m s^{-1} for S/N=100 from only 75 absorption lines observed at similar resolution of R=40,000. For spectra obtained at the lower S/N ratio, the photon-limited velocity errors increase linearly with the noise as in Eq. (5).

3.2 Wavelength Calibration Errors

The zero point of the wavelength scale is determined by fitting the observed iodine spectrum (superimposed on the stellar spectrum) with an iodine spectrum obtained from the Fourier-transform spectrometer (Valenti et al. 1995). We assume here that this FTS iodine spectrum has neither significant noise nor wavelength errors, at least relative to the errors caused by finite resolution and photons of our observed echelle spectra. The wavelength zero points are derived in the same way as the determination of the Doppler shifts, namely, by least-squares fitting of a model. Therefore, the photon-limited errors in the wavelength zero point so derived can be found just as was done above for the photon-limited errors in Doppler shift of the stellar spectrum. Here the relevant spectral slopes are those in the iodine spectrum after it has been convolved with the appropriate echelle PSF.

The resulting histogram of errors in the wavelength is given in Fig. 3 for S/N=200. Here, the errors' wavelength zero points have been translated into an effective velocity, using, $\epsilon_\lambda/\lambda=\epsilon_v/c$, with ϵ_v being the velocity error due to a wavelength error. Apparently the typical velocity error stemming from the uncertain wavelength zero point is about 30 m s^{-1} per chunk for S/N=200, comparable to the errors in the Doppler shift from the stellar spectrum alone.

These two errors (in wavelength and Doppler shift) are independent and Gaussian, and so propagate in quadrature within each chunk of spectrum. Combining all chunks with Eq. (6), the error in the mean velocity of the entire echelle spectrum from 5000 to 5800 Å (all chunks) is 1.8 m s^{-1}. This final error is composed of stellar Doppler error (1.2 m s^{-1}) and iodine-based wavelength error (0.9 m s^{-1}). Thus, in the absence of additional systematic errors (notably those due to the PSF), the intrinsic precision of Doppler measurements obtained with an iodine absorption cell at S/N=200 at resolution, R=60,000 is 1.8 m s^{-1}.

We have simulated observations of a T Tauri star by adopting τ Ceti as template and rotationally broadening it to simulate $V \sin i$=15 km s^{-1}. We add a constant 20% to the

actual continuum to simulate representative veiling of 20%. We add artificial Gaussian noise to simulate S/N ratio=30. Applying Eq. (6) to the entire T Tauri spectrum within the iodine region (5000–5800 Å) gives a photon-limited Doppler precision of 30 m s^{-1}, including both stellar shift and wavelength errors. Of course T Tauri stars may carry astrophysical limitations to velocity accuracy imposed by temporal variations in their spectra (Welty and Ramsey 1995).

3.3 Errors Caused by the Spectrometer PSF

Asymmetries in the spectrometer PSF will introduce systematic errors in Doppler measurements by imposing the asymmetry upon the shapes of the stellar line profile. This asymmetry will be interpreted as a "shift" in the absorption line by virtually any algorithm that is used to measure the Doppler shifts of lines. For example, the centroid of an absorption line will be shifted due to such an asymmetry. A cross-correlation or χ^2 minimization algorithm will similarly sense a PSF asymmetry and misinterpret it as a Doppler shift.

We estimate this error by considering a PSF that carries an asymmetry such that the centroid is displaced by some amount δ (in any units). Clearly, the convolution of this PSF with a narrow line (a delta function, say) will result in a displacement of exactly δ in the line. For convolution with broader lines, the resulting displacement is a complicated function of the linewidth and shape. Clearly, an asymmetric PSF will displace stellar lines and the (narrower) iodine lines by different amounts. Thus, an asymmetric PSF will cause spurious Doppler shifts in the stellar lines that are not compensated by an identical displacement in the wavelength scale derived from the iodine lines. A similar PSF-induced error will occur if any comparison spectrum is used, such as thorium lines to provide the wavelength scale.

This differential PSF effect on stellar and iodine lines is simulated by constructing an asymmetric PSF and convolving both a stellar and iodine spectrum with it. We fit the resulting skewed spectra with trial spectra that have no such asymmetry, with the free parameter being the spurious "shift" for best fit. As an example, we construct an asymmetric PSF by simply adding a displaced Gaussian to a symmetric Gaussian PSF.

For all 704 2-Å spectrum chunks in the region 5000–5800 Å for our Lick echelle spectra, we calculate the spurious shift for both the stellar and iodine spectra. The shift is calculated just as in the Doppler analysis, i.e., by χ^2 fitting of the skewed spectrum with the original spectrum. The difference between the stellar and iodine shifts is the net error due to the asymmetric PSF. The exercise reveals that a 1% PSF asymmetry causes spurious stellar and iodine shifts of about 24 and 20 m s^{-1}, respectively. The spurious shifts suffered by the stellar spectra are greater by 4.0 m s^{-1} systematically. Figure 4 shows the net shift, stellar minus iodine, in velocity units, thus simulating the net systematic error due to the PSF asymmetry.

It is clear that a systematic error of 4 m s^{-1} will accrue to Doppler measurements due to the relatively small variation in the PSF of 1%. This is a variation smaller than can be easily stabilized at the telescope. Even focusing the spectrometer to 1% FWHM seems difficult without extreme measures. Over time scales of years, it is doubtful that the PSF can be optically or mechanically forced to remain constant at the 1% level, given unforeseen optics changes. Therefore, the Doppler analysis and software must include both a measurement and accounting of the PSF with a precision of better than 1%, to keep errors under 4 m s^{-1}. Accordingly we derive a separate PSF for each 2-Å chunk of spectrum for each exposure (Valenti et al. 1995). A set of seven PSFs from a single exposure is displayed in Fig. 5, showing variability of several percent.

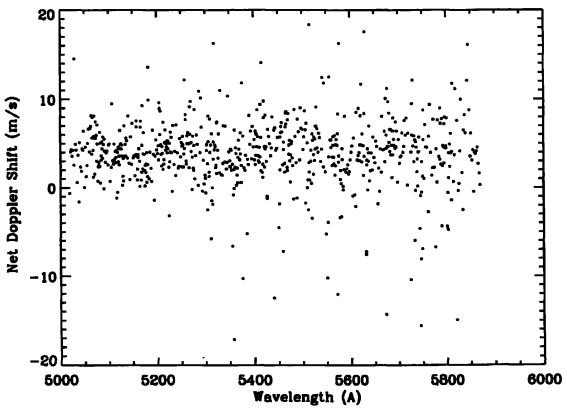

FIG. 4—The spurious net Doppler shift caused by a 1% asymmetry in the PSF. Each point represents the spurious Doppler shift in a 2 Å chunk of spectrum in τ Ceti. The stellar lines are systematically shifted by 4.0 m s^{-1} relative to those of iodine. This systematic error is removable by including the PSF in the Doppler analysis.

The quality of the derived PSF depends on the iodine line depth and S/N. The typical iodine line depth is observed to be ~20% at R=60,000. In iodine spectra that have S/N =100, each iodine line communicates the shape of the PSF with an effective S/N=20. Therefore, approximately 25 such

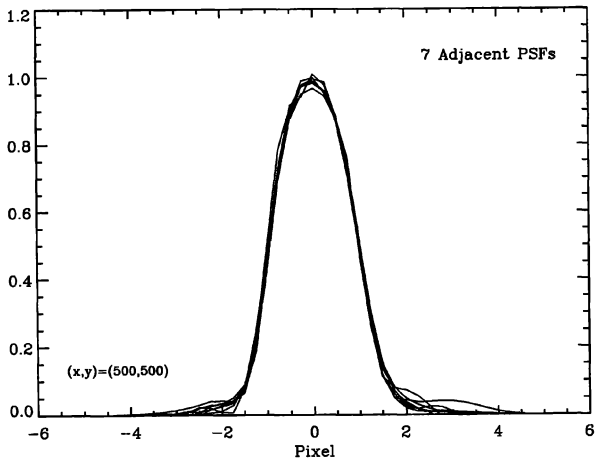

FIG. 5—Independently derived PSF profiles from seven adjacent regions in a CCD exposure of τ Ceti. These arise from the CCD domain at (row,col) =(500,500). The differences among the profiles represent errors in our ability to determine the PSF, since they all come from the same optical domain in the echelle format. The errors are apparently less than ~5%. In practice, the average of such a collection of PSFs in adopted to represent a domain to yield a superior PSF.

iodine lines are required to determine the PSF to an accuracy of 1%. In practice, we incorporate ~100 iodine lines to determine the local PSF within the echelle format. Thus the PSF is determined to a precision of ~0.5%, implying that velocity errors in each spectral chunk are ~2 m s^{-1}. This random velocity error is less than that due to photon statistics in each spectrum chunk, ~30 m s^{-1}, as discussed above. Therefore, the final velocity error from all wavelengths will remain as given in the above section on photon-limited errors, namely, ~2 m s^{-1}.

3.4 CCD Inhomogeneities

Precise Doppler measurements are affected by imperfections of the CCD chip. The individual pixels consist of potential wells that are neither uniform nor square, rendering imprecise any pixel binning during the construction of a synthetic model of the spectrum. As small, sub-pixel, Doppler shifts occur, such an internal pixel structure cannot be treated. Similarly, nonuniform spacing and sizes of pixels will mimic Doppler shifts as spectral lines cross those pixels. Flat-field calibration also suffers from nonuniform quantum efficiency within the pixel. Distortions in the flatness of the CCD affect the ability to achieve a uniform focus, and therefore affect the uniformity of the PSF.

Suppose that a CCD has pixel spacing errors of effectively 1%. For the dispersion of the Lick Hamilton echelle spectrometer of 2500 m s^{-1} per pixel, these CCD errors will induce Doppler errors of 1% of 2500 m s^{-1}=25 m s^{-1}. These Doppler errors must be local, since the dispersion is calculated over many pixels and will reflect large-scale variation in the pixel size. We therefore expect that local Doppler errors of 25 m s^{-1} will scatter both positively and negatively, as the local pixel spacing varies relative to its large-scale average. Thus, irregularities in pixel spacing may cause an additional Doppler error, comparable to photon-limited errors, assuming 1% spacing errors.

Similarly, Doppler errors due to nonuniform structure within the pixels themselves will induce local errors that cancel over large scales, i.e., will not cause systematic Doppler errors. However, it is difficult to estimate the magnitude of this quasirandom error. A pessimistic view is that a spot of light, spread over several pixels, will yield a centroid that is accurate to no better than, say, a few percent of pixel size, corresponding to ~100 m s^{-1} error locally. Techniques such as dithering the CCD could reduce such errors, but would cost valuable observing time.

3.5 Photospheric Turbulence

Searches for planets via Doppler measurements require that the center of mass of the star be measured. Unfortunately, the shapes of stellar absorption lines are not constant with time, exhibiting asymmetries that vary in velocity extent. These asymmetries are due to the line transfer through varying amounts of rising hot gas and falling cool gas within the photosphere. Such hydrodynamics may vary with phase of the stellar magnetic cycle which, on the Sun, has a period similar to that of Jupiter. Clearly, it may be difficult to disentangle such turbulent motion from true motion of the center of mass of the star. Typical flow velocities are ~300 m s^{-1} (Dravins 1985; Ulrich 1991). The question arises regarding the degree to which such velocities "average out" over a stellar disk and whether the ultimate limitation of precise velocity measurements lies in the variation of line profiles with stellar magnetic cycle.

McMillan (1993) reviews this issue and finds no trend in measured radial velocities of the integrated disk of the Sun (using the Moon) during 5 years. He finds a limit of ±4 m s^{-1} using lines in the blue portion of the spectrum. This limit is $\frac{1}{3}$ of the signal Jupiter induces, thus ensuring that similar stars would be amenable to detection of Jupiter-like planets. Alternatively, Jimenez (1986), working in the strong potassium line in the near IR, saw a 15 m s^{-1} variation during a solar cycle. The large variation may reflect hydrodynamic effects at the upper photospheric heights that are not sampled with optical lines of medium strength. Most relevant to iodine work is the report by Wallace et al. (1988) whose Doppler measurements of the Sun were made with neutral Fe lines near 5300 Å. They find no modulation greater than their threshold of detectability of 6.5 m s^{-1}. Harvey (1985) has estimated the noise due to convection will be 3 m s^{-1} short term. Walker et al. (1995) find velocity variations of ~20 m s^{-1} in the chromospherically active stars ϵ Eridani and ξ Boo A, suggesting possible turbulent origin.

Gray and Baliunas (1994) have measured the line asymmetries in τ Ceti for 9 years and find marginal evidence of a trend. The *span* of the line profile bisectors may vary by 4 m s^{-1} per year. But it is not clear whether a changing line span translates into a spurious Doppler shift of the line. Our measured velocities for τ Ceti vary by no more than 8 m s^{-1} during 7 years. One solution is to measure variations in the line asymmetries in τ Ceti to correct or correlate with ensuing Doppler errors, if any. Precise Doppler measurements should be accompanied by chromospheric diagnostics to monitor magnetic cycles. We do monitor several chromospheric indicators, namely, Hα and the Ca II IR triplet to expose correlations between activity and measured velocity. Such correlations would cast severe doubt on the interpretation of the Doppler shifts (Larson et al. 1993).

4. PRECISION VELOCITY TESTS

As a test of the radial-velocity technique, a series of day-sky observations were made on 1995 March 24 with the Hamilton spectrometer. The CAT telescope was simply pointed toward the zenith, thereby acquiring scattered day-sky light. Twenty-four sets of three observations each were taken over 5 hr. The odd-numbered sets were taken in the nominal spectrometer setup, using a 600μ slit and normal focus. For the even-numbered sets, the spectrograph was purposely adulterated to stimulate grotesque long-term optical or mechanical variations in the spectroscopic performance. The day-sky spectra were then analyzed for Doppler shifts in the usual way. After correction for Earth's rotational velocity, these Doppler shifts should all be identical.

The actual day-sky results are shown in Fig. 6. The velocity trend due to the Earth's rotation has been removed. The nominal observations are indicated with boxes and adulterated observations with dots. The scatter of the 36 nominal

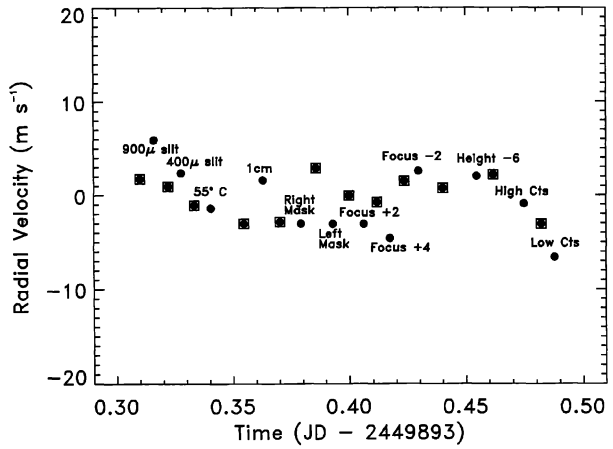

FIG. 6—Day-sky test. The Hamilton spectrometer was intentionally adulterated during a 5-hr string of day-sky observations to mimic long-term variations in the spectrometer performance. All points are the average of three exposures. The boxed points are nominal "reference" observations. With the exception of using a very large slit (900μ), none of the spectrometer variations led to a systematic error greater than 3 m s^{-1}.

observations is 2.7 m s^{-1}. Apparently, our random errors are 2.7 m s^{-1}, nearly consistent with the expected photon-limited errors of 2 m s^{-1} discussed in Sec. 3.2 for S/N=200. When binned in groups of three exposures per bin, the scatter in the velocities falls to 2.1 m s^{-1}. To identify systematic errors, Fig. 6 displays the average velocity within each set of three exposures. We interpret the apparent differences to suggest that systematic errors remain in our technique at a level of ~1 m s^{-1}, which must be corrected in future analyses.

The labels on Fig. 6 indicate how the spectrograph was adulterated for each of the non-nominal observations. In the first such set, the slit was widened 50% to 900 μ. This set appears systematically high by 6 m s^{-1}, indicating a serious error which is not accommodated by our PSF description. Future PSF descriptions will treat this possibility. However, this is not a long-term problem since such a large slit will never be used in the precision velocity program.

The other non-nominal setups include using a 400μ slit, moving the iodine absorption cell by 1 cm, placing a mask over the right and left edges of the collimating mirror, intentionally de-focusing the spectrograph by 2 and 4 units (focus precision is ±1 unit), displacing the CCD by roughly one pixel (Height-6), taking exposures near the saturation limit of the CCD (High Cts), and taking exposures with low S/N (≈30), labeled "Low Cts." None of these adulterations of the spectrometer caused an apparent systematic error in the derived velocity of the day sky by more than 3 m s^{-1}. The rms scatter of the full data string of 72 observations is 3.0 m s^{-1}. We conclude that long-term changes in the spectrometer will cause errors of no greater than 3 m s^{-1}.

Figure 7 shows the first year of "post-fix" radial-velocity data for τ Ceti (HR 509, HD 10700, G8 V, V=3.50). This star has previously been determined to be among the most stable stars known (Campbell et al. 1988; Walker et al. 1995). The rms scatter in the measured radial velocities is 4.6 m s^{-1}. Most of these observations have been made on the 0.6-m Coudé Auxiliary Telescope (CAT), and these observations typically have the largest error bars due to lower S/N compared to the observations made with the 3-m Shane Telescope. The typical S/N ratio of the 3-m observations is 300, while the Coudé Auxiliary Telescope provides a S/N ratio of 100 to 200. The relatively large scatter of 4.6 m s^{-1} is due to the random errors of the low S/N CAT observations.

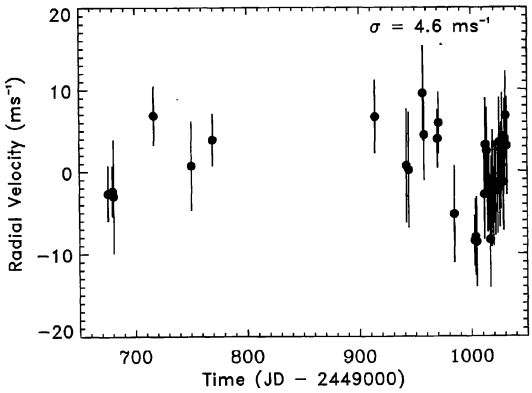

FIG. 7—One year of radial velocities for τ Ceti (G8 V). The rms scatter of these velocities is 4.6 m s^{-1}.

τ Ceti is the brightest star in the Lick Iodine Planetary Survey sample. At 3 magnitudes fainter, HR 1614 (HD 32147, K3 V, V=6.22) is more typical of our sample. We have obtained four observations over the last year, all on the 3-m Shane Telescope. Figure 8 shows the resulting velocities. The average internal error of the individual observations is 3.7 m s^{-1}, while the rms scatter of the observations is 2.2 m s^{-1}. The precision of these observations may be helped by virtue of the fact that all observations were made on the same telescope, thus minimizing PSF variations.

Figures 6–8 show that the current analysis package is immune to systematic errors at the level of 3 m s^{-1} both over the long term and due to a wide variety of potential insults that the Hamilton might suffer. Figure 9 shows an example of the run-to-run variation in the PSF of the Hamilton that our analysis package is able to model out in the post-fix era. The solid line is the PSF determined from an observation of τ Ceti made through the iodine cell on the night of 1994 November 18/19 with the 3-m Shane Telescope. The dotted

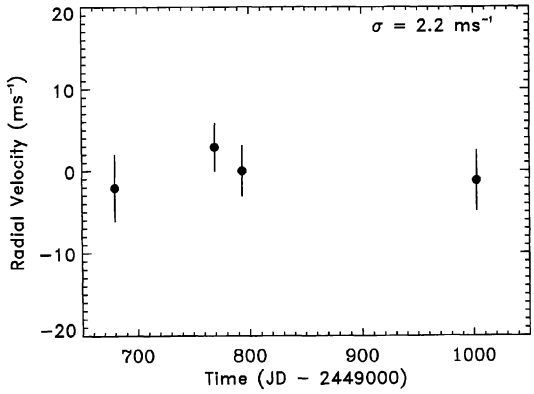

FIG. 8—One year of radial velocities for HR 1614 (K3 V). The rms scatter of these velocities is 2.2 m s^{-1}.

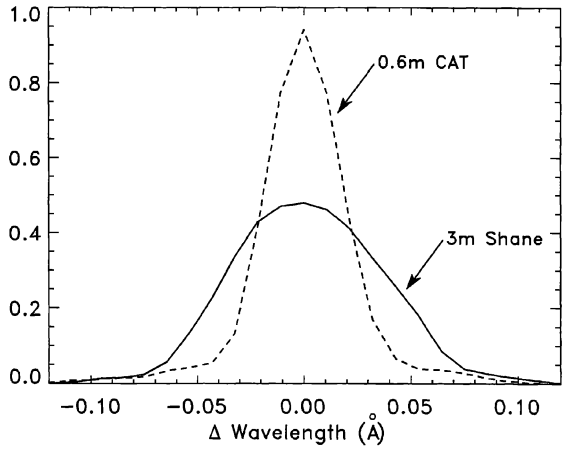

FIG. 9—The Hamilton spectrometer PSF. The solid line is the derived PSF from 1994 November, with the 3-m Shane Telescope. The dashed line is from 1995 September, with the 0.6-m Coudé Auxiliary Telescope. These variations in PSF are included in the determination of Doppler shifts.

line is the PSF determined from an observation of τ Ceti made 1995 September 8/9 with the 0.6-m CAT. The PSF for the latter observation is much sharper.

The need to achieve a S/N ratio of 300 limits the stars that the 3-m Shane Telescope can survey to those brighter than $V=8$. There are very few K and M dwarfs this bright. Any attempt to survey more stars, in particular, K and M dwarf stars, will require the use of a large telescope. Toward this end we have constructed an iodine absorption cell for the HIRES Spectrograph on the Keck I Telescope. During a HIRES commissioning night on 1993 October 1 a string of 200 observations of the K dwarf 107 Psc (HR 493) was obtained over 6 hr. The results of this run are shown in Fig. 10. The rms scatter of these velocities is 3.2 m s^{-1}, indicative of the Doppler error. This was one of the initial observing runs with the Keck, and conditions were less than optimal. In particular, the primary mirror segments did not align as well as they have subsequently come to do. The first gap in the data is due to an attempt to refocus the telescope. The second gap is due to the star passing through the zenith singularity of the azimuth drive.

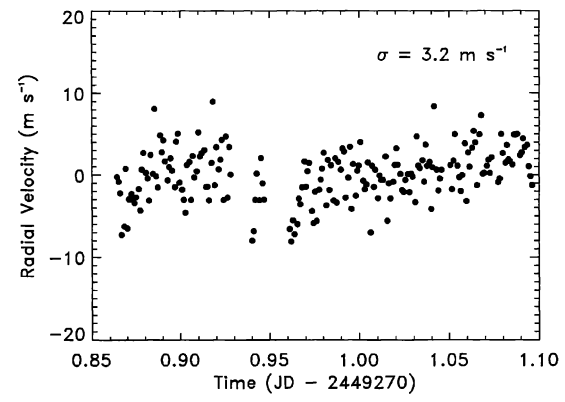

FIG. 10—Seven hours of Keck HIRES radial-velocity data for 107 Psc (K1 V). The rms scatter of these velocities is 3.2 m s^{-1}.

5. DISCUSSION

We have constructed a combined system of spectroscopic hardware and an analysis package that achieves Doppler errors of ~3 m s^{-1} for spectra having S/N ratio=200. A further error estimate comes from 103 spectra, having a S/N ratio of only 100, of 51 Peg (G4 V). This star exhibits sinusoidal velocity variations with a 4.23-d period and 56 m s^{-1} amplitude, with residuals of 5 m s^{-1} (Mayor and Queloz 1995; Marcy and Butler 1996). We interpret these 5 m s^{-1} residuals as upper limits to the errors that arise from low S/N, but consistent with the 3 m s^{-1} errors that are achieved for S/N=200.

We find that long-term errors are held to 3 m s^{-1}, while the estimated error budget (Sec. 3) predicts errors of only 2 m s^{-1}. Therefore, systematic errors do persist in our Doppler technique at a level of 1 m s^{-1}. These systematic errors are also apparent in the imperfect model fits to observed spectra: the reduced χ^2 statistic is typically 1.5, instead of 1.0 as would be expected for purely photon-limited errors. Our actual errors are 50% larger than dictated by photon statistics alone. The most likely source of this error resides in imperfect deconvolution of the PSF from our reference "template" stellar spectra. Future improvements should include higher-resolution spectra and superior description of the PSF.

We continue to pursue techniques which will further reduce systematic errors. Such ideas include the application of nightly corrections (Campbell and Walker 1988) and increasing the model oversampling from a factor of 4 to 8. Our goal is to achieve a photon-limited precision of 1 m s^{-1}. This will require the use of a 10-m "Keck" class telescope to acquire observations with S/N ratios in excess of 500.

A number of improvements are planned for the Hamilton spectrometer. An automated liquid-N_2 feed will be installed to feed the CCD dewar to decrease the traffic in the Coudé camera room. A tip-tilt system at the spectrometer slit entrance would increase the number of photons that go through the slit by as much as a factor of 2. A thinned CCD would further increase the photon efficiency of the system by a factor of 2. These improvements would double the S/N of observations for a given exposure time. Temperature stabilizing the Coudé camera room would minimize changes in the spectrometer PSF. A fiber-optic coupler at the slit would be desirable to maintain constant PSF, but only if it had high throughput.

The HIRES could also use two improvements to facilitate precision velocity observations: (1) an operator-controlled spectrometer focus mechanism, and (2) a CCD with smaller pixel size. The resolution of HIRES is currently limited by the 24μ pixel size. The precision of the radial-velocity measurements would be improved by about 25% if a CCD with 15μ pixels were used.

Finally, the modeling technique described in this paper (and Valenti et al. 1995) requires a significant CPU commitment. Approximately 2 CPU hours on a Sparc10 class machine are required to analyze each observation. The HIRES data set shown in Fig. 10 took 3 CPU weeks to analyze. We believe that there may be systematic errors at the 2 m s^{-1} level in these results. This analysis was carried out in 1995

May. Since then, numerous subtle improvements have been made to the analysis package. If this data set were to be reanalyzed we expect the scatter would be decreased. We are in the process of obtaining more and faster computers to carry out the modeling.

A debt of gratitude is owed to Jeff Valenti for his work on the "Hamilton spectrometer" reduction package and the spectrometer PSF recovery routine. The long-term stability of the iodine cell is a tribute to the glassblowing skills of Mylan Healy. Thanks are owed to the entire staff at Lick Observatory, especially Anthony Misch for perfecting the Hamilton Schmidt camera optics. Wayne Earthman built a "photon-weighted" exposure meter. The reference spectrum of the iodine absorption cell was determined with the assistance of Claude Plymate at Kitt Peak National Observatory, using the Fourier Transform Spectrometer at the McMath Solar Telescope. This research has been supported by NASA Grant No. NAGW 3183.

REFERENCES

Brown, T. M., Noyes, R. W., Nisenson, P., Korzennik, S. G., and Horner, S. 1995, PASP, 106, 1285
Butler, R. P. 1987, Master's thesis, San Francisco State University
Butler, R. P. 1992, ApJ, 394, L25
Butler, R. P. 1993, ApJ, 415, 323
Campbell, B., Walker, G. A. H., and Yang, S. 1988, ApJ, 331, 902
Cochran, W. D., and Hatzes, A. P. 1994, in Planetary Systems: Formation, Evolution, and Detection, ed. B. F. Burke, J. H. Rahe, and E. E. Roettger (Dordrecht, Kluwer), p. 281
Deming, D., Espenak, F., Jennings, D. E., Brault, J. W., and Wagner, J. 1987, ApJ, 316, 771
Dravins, D. 1985, in Stellar Radial Velocities, IAU Colloquium No. 88, ed. A. G. Davis Phillip and D. Latham, pp. 311–320
Gilliland, R. L., Morris, S. L., Weymann, R. J., and Ebbets, D. C. 1992, PASP, 104, 367
Griffin, R. 1973, MNRAS, 162, 243
Hatzes, A., and Cochran, W. D. 1995, ApJ, preprint
Hearnshaw, J. B. 1993, in Seeking Other Planetary Systems: The Role of Stellar Radial Velocity Measurements, workshop held at the Harvard Smithsonian Center of Astrophysics, June 1992, ed. Latham, Cochran, McMillan, p. II-355
Horner, S. 1993, in Seeking Other Planetary Systems: The Role of Stellar Radial Velocity Measurements, workshop held at the Harvard Smithsonian Center of Astrophysics, June 1992, ed. Latham, Cochran, McMillan, p. II-217
Jimenez, A., et al. 1986, Adv. Space Res., 6, 89
Jimenez, A., et al. 1988, in Advances in Helio- and Asteroseismology, IAU Symposium 123, ed. J. Christensen-Dalsgaad and S. Frandsen (Dordrecht, Reidel), p. 215
Koch, A., and Wohl, H. 1984, A&A, 134, 134
Larson, A. M., Irwin, A. W., Yang, S. L. S., Goodenough, C., Walker, G. A. H., Walker, A. R., and Bohlender, D. A. 1993, PASP, 105, 332
Libbrecht, K. G., and Peri, M. L. 1995, PASP, 107, 62
Marcy, G. W., and Butler, R. P. 1992, PASP, 104, 270
Marcy, G. W., and Butler, R. P. 1996, ApJL (submitted)
Mayor, M., and Queloz, D. 1995, Nature, 378, 355
McCarthy, C. 1995, Master's thesis, San Francisco State University
McMillan, R. S., Moore, T. L., Perry, M. L., and Smith, P. H. 1994, in Planetary Systems: Formation, Evolution, and Detection, ed. B. F. Burke, J. H. Rahe, and E. E. Roettger (Dordrecht, Kluwer), p. 271
McMillan, R. S., Moore, T. L., Perry, M. L., and Smith, P. H. 1993, ApJ, 403, 801
Merline, W. J. 1985, in Stellar Radial Velocities, IAU Colloquium No. 88, ed. A. G. Davis Philip and D. W. Latham (Schenectady, Davis), p. 87
Press, W. H., Flannery, B. P., Teukolsky, S. A., and Vetterling, W. T. 1986, Numerical Recipes (Cambridge, Cambridge University Press), p. 19
Ramsey, L. W. 1987, in Fiber Optics in Astronomy, ed. S. C. Barden, ASP Conf. Series 3, p. 26
Standish, E. M., Newhall, X. X., Williams, J. G., and Folkner, W. F. 1995, JPL Planetary and Lunar Ephemerides, DE403/LE403, JPL IOM 314.10, 127
Standish, E. M. 1990, A&A, 233, 252
Taylor, J. R. 1982, in An Introduction to Error Analysis, ed. E. D. Commins, p. 128
Ulrich, R. K. 1991, in Adv. Space Res. (COSPAR), 11, 217
Valenti, J. A., Butler, R. P., and Marcy, G. W. 1995, PASP, 107, 966
Vogt, S. S. 1987, PASP, 99, 1214
Vogt, S. S., et al. 1994, Proc. Soc. Photo-Opt. Instrum. Eng., 2198, 362
Walker, G. A. H., Walker, A. R., Irwin, A. W., Larson, A. M., Yang, S. L. S., and Richardson, D. C. 1995, Icarus, 116, 359
Wallace, L., Huang, Y. R., and Livingstone, W. 1988, ApJ, 327, 399
Welty, A. D., and Ramsey, L. W. 1995, AJ, 110, 336